

Molecular Dynamics Simulation of Thermal Boundary Conductance Between Carbon Nanotubes and SiO₂

Zhun-Yong Ong^{1,2} and Eric Pop^{1,3,4}

¹*Micro and Nanotechnology Lab, Univ. Illinois at Urbana-Champaign, Urbana IL 61801, U.S.A.*

²*Dept. of Physics, Univ. Illinois at Urbana-Champaign, Urbana IL 61801, USA*

³*Dept. of Electrical & Computer Engineering, Univ. Illinois at Urbana-Champaign, Urbana IL 61801, USA*

⁴*Beckman Institute, Univ. Illinois at Urbana-Champaign, Urbana IL 61801, USA*

We investigate thermal coupling between carbon nanotubes (CNTs) and SiO₂ with non-equilibrium molecular dynamics simulations. The thermal boundary conductance (G) per unit length is found to scale with the strength of the Van der Waals interaction ($\sim\chi$), with CNT diameter ($\sim D$), and as a weak power law of temperature ($\sim T^{1/3}$). The thermal relaxation time of a single CNT on SiO₂ is independent of diameter, $\tau \approx 85$ ps. With the standard set of parameters $G \approx 0.1$ W K⁻¹ m⁻¹ for a 1.7 nm diameter CNT at room temperature. Our results are comparable to, and explain the range of experimental values for CNT-SiO₂ thermal coupling from variations in diameter, temperature, or details of the surface interaction strength.

Contact: epop@illinois.edu

PACS numbers(s): 65.80.-g, 61.46.Fg, 68.35.-p, 68.47.Gh

I. INTRODUCTION

Energy transport across the interfaces of nanostructures and their surrounding medium plays a critical role in the performance and stability of carbon nanotubes (CNTs), graphene nano-ribbons, or other nanomaterials. For instance, thermal transport through CNT composites is dominated by the small interface thermal conductance,^{1,2} rather than the large intrinsic thermal conductivity of the nanotubes themselves.³⁻⁵ The thermal conductance of CNT arrays with potential heat sinking applications is similarly restricted at the interface with the silicon chip substrate (Fig. 1a).^{6,7} In CNT transistors and interconnects, the maximum current-carrying ability of the devices appears limited by self-heating and heat dissipation with the dielectric substrate (Fig. 1b).^{8,9} In all these cases, heat dissipation from the CNTs to the environment is determined by the thermal boundary conductance (TBC) at their interface. In particular, the nanoscale constriction between the CNT and the substrate or environment, combined with the weak bonds at this interface are expected to lead to a small TBC.^{10,11}

In this context, it remains highly desirable to examine the atomistic details of the nanotube-substrate thermal coupling in order to understand the different channels of heat dissipation. Moreover, the dependence of TBC on nanotube diameter, temperature, and Van der Waals interaction strength are presently unknown. In addition, the predominant dielectric within integrated circuits is SiO_2 , which also forms a thin surface layer (native oxide) on the backside of silicon chips where CNT heat sinks would be attached. Thus, the primary goal of this paper is to investigate the lattice (phonon) contribution to the TBC between single-walled carbon nanotubes and amorphous SiO_2 using the molecular dynamics (MD) simulation technique. The MD technique has been previously used to examine the TBC between nanotubes and surrounding liquid or solid media.¹²⁻¹⁶ Here, we study the TBC with SiO_2 as a function of the substrate temperature as well as the interaction strength between the substrate and the CNT. We also examine the dependence of the TBC on diameter in armchair nanotubes. Finally, we compare our results with existing thermometry data for the TBC of CNTs on SiO_2 substrates.¹⁷⁻¹⁹

II. MOLECULAR DYNAMICS SETUP

We begin with a brief description of the MD simulation technique. MD treats the atoms in the system classically. The atoms are modeled as point masses and, for a given set of interatomic potentials for the different species of atoms, the equation of motion for atom i can be written as

$$m_i \ddot{\vec{r}}_i = \sum_{j \neq i} \vec{f}_{ij} \quad (1)$$

where \vec{r}_i is its position, m_i its mass and \vec{f}_{ij} the force between it and atom j . The equations of motion are then integrated numerically to produce the classical trajectories of the system. To perform our simulations, we use the MD code LAMMPS²⁰ because of its parallelization and the implementation of the interatomic potentials used. Our simulations were run on a Linux cluster which consists of eight 3.0 GHz CPU cores (Intel 5400 series) with 16 GB of memory.

A. Description of CNT and SiO₂

To model the interactions between carbon atoms (C-C) in the molecular dynamics simulation, we use the adaptive intermolecular reactive empirical bond order (AIREBO) potential²¹ derived from the second generation Brenner potential.²² The AIREBO potential is widely used in MD simulation of CNTs and has been implemented in LAMMPS. The AIREBO potential also reproduces the phonon density of states (DOS) accurately, with a cutoff at approximately 56 THz, as shown in Fig. 1c.

To model the Si-Si, Si-O and O-O atomic interactions, we use the recently published Ter-soff-type potential parameterization of Si-O systems by Munetoh,²³ which we will henceforth refer to as the Munetoh potential. The Munetoh potential reproduces the vibrational DOS of bulk amorphous SiO₂ in good agreement with known experimental data.²⁴ The structure of the amorphous SiO₂ produced with the Munetoh potential has been shown to be that of a three-dimensional random network of SiO₄ tetrahedral units.^{23, 25} The vibrational DOS for the Si and O atoms in the substrate are also shown in Fig. 1c, noting that Si and O phonon spectra do not extend beyond 40 THz. Although our choice of interatomic potentials for SiO₂ does not take into account long-range Coulombic interaction, this is less likely to matter for the problem at hand as the interfacial thermal transport depends only on the Van der Waals (VdW) interaction between the CNT and substrate atoms. The main consideration in our choice of the interatomic potentials for the nanotube and the substrate is the realism of the vibrational DOS of the simulated atoms.

B. Interaction between CNT-SiO₂

There is some uncertainty in the strength and form of the interactions between the CNT atoms and the substrate atoms. It has been proposed that the interaction between the CNT and

substrate is primarily Van der Waals.²⁶ Thus, the Si-C and O-C interactions are modeled as weak VdW interactions using the 12-6 Lennard-Jones (LJ) potential function, written as

$$V(r) = 4\chi\epsilon \left[\left(\frac{\sigma}{r} \right)^{12} - \left(\frac{\sigma}{r} \right)^6 \right] \quad (2)$$

where ϵ is the energy parameter, σ the distance parameter, r the interatomic distance and χ is a scaling factor. The ϵ parameters determine the strength of the specific interactions between the nanotube and the substrate atoms. We have two ϵ parameters ($\epsilon_{\text{Si-C}}$ and $\epsilon_{\text{O-C}}$) and two σ parameters ($\sigma_{\text{Si-C}}$ and $\sigma_{\text{O-C}}$). The general scaling factor χ adjusts the overall nanotube-substrate interaction. The parameters used in our simulations are based on those for VdW interactions in the Universal Force Field (UFF) model by Rappe et al.²⁷ The UFF-based parameters are $\epsilon_{\text{Si-C}} = 8.909$ meV, $\epsilon_{\text{O-C}} = 3.442$ meV, $\sigma_{\text{Si-C}} = 3.326$ Å and $\sigma_{\text{O-C}} = 3.001$ Å. The parameters are calculated using the Lorentz-Berthelot mixing rules.²⁸ The cut-off distances for the LJ potential for the Si-C and O-C interactions are set to 8.315 Å and 7.503 Å respectively. To study the effect of the substrate-CNT interaction strength, we repeat our simulations with different values of χ . We use $\chi = 1, 2$ and 4 for the scaling factor in the simulations, with $\chi = 1$ corresponding to the original form of the LJ interactions as used in the UFF.

C. Preparation of Simulation Domain

The nanotube-substrate domain is prepared as shown in Fig. 2. It is relevant to point out we focus on the “horizontal” nanotube-SiO₂ interaction, as opposed to the vertical case which has been previously studied for nanotube-Si thermal transfer.^{15, 16} We believe the horizontal scenario is more relevant to heat dissipation from CNTs in both heat sink applications as well as interconnects, as shown in the schematics of Fig. 1a and Fig. 1b. Even for vertical CNT arrays with potential heat sink applications,^{6, 7} the CNTs contacting the substrate will most likely do so at a “bent” angle, more consistent with the lateral coupling studied here. Moreover, silicon wafer substrates are typically covered with a thin, native SiO₂ layer (1-2 nm thick), such that the relevant interfacial atomic interaction is that between the CNTs in the array and the surface SiO₂.

To build the amorphous SiO₂ layer we first replicate a β-cristobalite unit cell within a rectangular simulation domain of 57.3 × 28.7 × 36.9 Å with periodic boundary conditions in all three directions. To obtain the amorphous bulk SiO₂, we anneal the crystalline SiO₂ atoms at the

temperature of 6000 K for 10 ps and at fixed pressure of 1 bar using a time step of 0.1 fs. Then, we slowly quench the structure to 300 K at a rate of 10^{12} K/s. To create the SiO_2 surface from the amorphous structure, the silica atoms in the top half of the simulation domain are deleted to obtain an amorphous SiO_2 slab with 3904 atoms. Using the conjugate gradient algorithm, we perform an energy minimization of the resultant structure to produce the final SiO_2 surface. A 36.9 Å long, 600-atom (10,10) CNT was constructed and inserted into the top half of the simulation domain just above the amorphous SiO_2 slab. Once again, we perform an energy minimization to obtain the final substrate-CNT structure shown in Fig. 2.

III. SIMULATION OF CNT-SUBSTRATE THERMAL COUPLING

The phonon density of states (DOS) of the carbon nanotube and SiO_2 substrate are proportional to the Fourier transform of the velocity autocorrelation function (VACF). The normalized velocity autocorrelation function (VACF) of an atom can be written as

$$f(t) = \frac{\langle \vec{v}(0) \cdot \vec{v}(t) \rangle}{\langle \vec{v}(0) \cdot \vec{v}(0) \rangle} \quad (3)$$

where $\vec{v}(t)$ is the velocity of the particle at time t and the angled brackets $\langle \dots \rangle$ represent the ensemble averages. For long simulation times, the ensemble averages can be replaced by the time averages. The calculated phonon (vibrational) DOS of the C atoms in the CNT and the Si and O atoms in the substrate are shown in Fig. 1c.

Once the density of states is known it is necessary to define a local temperature T . We use the ‘kinetic’ definition for an atomistic system as

$$T = \frac{1}{3Nk_B} \sum_{i=1}^N m_i v_i^2 \quad (4)$$

where N is the number of atoms in the system, m_i the mass of the i -th atom and v_i its velocity. In order to simulate the interfacial heat transfer, we have to set up an initial temperature difference ΔT between the CNT and substrate atoms, with the CNT at the higher temperature. In the absence of additional coupling to an external heat reservoir, ΔT decays exponentially with a single relaxation time τ i.e.

$$\Delta T(t) = \Delta T(0) \exp\left(-\frac{t}{\tau}\right). \quad (5)$$

Given that the thermal resistance of the nanotube-substrate interface is much greater than the internal thermal resistance of the nanotube, we can apply a lumped heat capacity method, as schematically shown in the Fig. 2d inset. Thus, the thermal boundary conductance (TBC) per unit nanotube length (G) is given by

$$G = \frac{C_{CNT}}{\tau} \quad (6)$$

where C_{CNT} is the heat capacity per unit length of the nanotube. We use the definition of TBC per unit length rather than the more conventional conductance per unit area²⁹ because the contact area between the CNT and substrate is not easily defined. However, the latter could still be approximated by normalizing G through the CNT diameter, as we do later in Fig. 6 and surrounding discussion. In our simulations, we set the CNT-substrate temperature difference ΔT to be a fraction of the initial substrate temperature. If ΔT is too small with respect to the substrate temperature, the relaxation process will be very noisy. On the other hand, if ΔT is too large with respect to the substrate temperature, it becomes difficult to determine the temperature dependence of the TBC. As a compromise, we set ΔT to be 50 percent of the initial substrate temperature.

In order to produce the temperature difference between the CNT and the substrate, we equilibrate the atoms in the CNT and the top four-fifths of the slab in Fig. 2d at the desired temperature T for 100 ps. The atoms in the bottom fifth of the slab are always kept frozen (motionless) to anchor the substrate. The atoms are set to a given temperature using velocity rescaling with a time step of 0.25 fs. Afterwards, the velocity rescaling algorithm is switched off and the system is allowed to equilibrate. To produce a temperature difference between the CNT and substrate, we again apply the velocity rescaling algorithm to the substrate atoms at the temperature T and to the CNT atoms at temperature $T+\Delta T$ for 10 ps.

To simulate the heat transfer process, the velocity rescaling is switched off and the system is allowed to relax. We then record the decay of the temperature difference between the nanotube and the substrate. Because this temperature decay ΔT is noisy, it is necessary to average over multiple runs (ten in our case) to obtain the exponential decay behavior as shown Fig. 3a and 3b, and expected through the lumped model from Eq. (5). Throughout this work, we repeat such simulations for several Van der Waals strength scaling factors ($\chi = 1, 2$ and 4), and typical temperature decay plots are shown in Fig. 3a and 3b. Moreover, the cross-sectional profile of a (10,10)

nanotube on SiO_2 is shown for the three interaction strengths in Fig. 3c. As expected, the CNT profile becomes progressively deformed as the interaction strength increases. The minimum CNT- SiO_2 equilibrium separation is found to be approximately 2.2 Å, in close agreement with a recent density functional theory (DFT) study of the CNT-quartz interaction,³⁰ which found a separation of 2.5 Å.

IV. SIMULATION RESULTS

A. Temperature Dependence of TBC

We perform our simulations at different substrate temperatures ($T = 200, 300, 400, 500$ and 600 K) with different VdW strength scaling factors ($\chi = 1, 2$ and 4). Figure 4a shows our calculations of the thermal boundary conductance for the (10,10) nanotube interface with the amorphous SiO_2 substrate. The results show that the TBC increases monotonically both with temperature and with VdW coupling strength χ . The temperature dependence of the TBC for the horizontal CNT is consistent with the temperature dependence of TBC for vertically aligned CNTs¹⁶ with Si substrates, and other simulations.³¹ At higher temperatures, more phonons are excited in the CNT and the substrate and are able to participate in interfacial thermal transport.

To further clarify the dependence of the TBC on temperature, the results at different temperatures normalized by the TBC at 200 K are plotted in Fig. 4b. We find that the temperature dependence is remarkably similar for all values of interaction strength χ considered. For example, the TBC at 600 K is roughly 40 percent greater than the TBC at 200 K. This implies that the TBC scales with temperature independently of its interaction with the substrate and suggests that there may be a simple power law behavior in terms of scaling with respect to temperature. The data are in good agreement with a $T^{1/3}$ fit over this temperature range, as shown in Fig. 4b.

B. Interaction Strength Dependence of TBC

To determine the effect of the CNT-substrate interaction strength (χ) on the thermal boundary conductance, we replot the TBC results rescaled by $1/\chi$ in Fig. 4c. These results suggest that the TBC is directly proportional to the substrate-CNT interaction strength, in contrast to the conventional diffuse and acoustic mismatch models (DMM and AMM)³² which do not capture the atomistic interaction and atomic arrangement at the interface. It should also be noted that the DMM and AMM are usually applied to dissimilar *bulk* materials and are not necessarily ex-

pected to produce good agreement for nanomaterial interfaces. Thus, atomistic molecular dynamics investigations, such as the present work, are essential in exploring and explaining heat and energy transfer across the interfaces of carbon nanotubes and other nanomaterials.¹²⁻¹⁶

This particular outcome can be better understood by considering the interatomic coupling of CNT and substrate atoms. In the harmonic limit, the energy of the p -th atom can be written as

$$E_p = \frac{1}{4} \sum_q (u_p^* H_{pq} u_q + u_q^* H_{qp} u_p) + \frac{1}{2} M_p \ddot{u}_p^* \ddot{u}_p \quad (7)$$

where u_p and M_p are the displacement and mass of the p -th atom, and H_{pq} is the second derivative of the interatomic potential i.e.

$$H_{pq} = \frac{\partial^2 \phi}{\partial u_p \partial u_q} \quad (8)$$

and ϕ is the interatomic potential. If we take the time derivative of E_p , use Newton's second law

$$M_p \ddot{u}_p = - \sum_q H_{pq} u_q \quad (9)$$

and sum over the atoms in the CNT, then we obtain following expression

$$\sum_p \frac{dE_p}{dt} = \frac{1}{4} \sum_p \sum_q (u_p^* H_{pq} \dot{u}_q + \dot{u}_q^* H_{qp} u_p - u_q^* H_{qp} \dot{u}_p - \dot{u}_p^* H_{pq} u_q) \quad (10)$$

where the sum over p is for the CNT atoms and the sum over q is for the substrate atoms. The H_{pq} terms that survive in Eq. (10) correspond to the second derivative of the LJ interaction between the CNT and the substrate and scale linearly with χ as given in Eq. (2). Thus, as we increase χ , the rate of energy dissipation from the CNT atoms to the substrate atoms increases proportionally. As a result, the decay time τ varies inversely with χ , as we have seen in Fig. 3. Therefore the TBC scales proportionally with χ , because increasing the latter also increases the harmonic coupling between the phonons modes in the CNT and the substrate.

The dependence of the TBC on the substrate-nanotube interaction strongly suggests that a simple strategy for engineering this thermal coupling would be to modify the atomic species on the surface of the substrate. For example, if the surface is passivated with a relatively inert species that does not interact strongly with carbon, then the TBC will decrease. Alternatively, if the

surface roughness is increased so that the overall physical contact between the nanotube and the substrate is reduced, then the TBC will also decrease. Conversely, by improving the surface smoothness, e.g. along the steps of a miscut crystalline insulating substrate, the TBC should be improved. Similarly, functionalizing nanotubes with polymers or metals that increase both coupling strength, phonon DOS overlap, as well as interaction area should also lead to improved TBC.³³

C. Diameter Dependence of TBC

To study the diameter dependence of the TBC, we repeat our simulations with armchair CNTs of (6,6), (8,8), and (12,12) chirality, corresponding to diameters of 0.81, 1.08 and 1.63 nm, respectively. The setup is identical to our earlier simulation with the (10,10) nanotube except for the size of the system. The cross sections of the CNTs are shown in Fig. 5. The substrate-CNT interaction scaling factor is maintained at $\chi = 1$. The nanotubes are all approximately 98.4 Å long and between 8.1 and 16.3 Å in diameter. In each run, the substrate and the CNT atoms are equilibrated at 300 K and 500 K, respectively, for 80 ps using velocity rescaling before the temperature difference between the CNT and the substrate is allowed to decay over 80 ps. We average the temperature decay over five runs for each CNT. As before, the decay time is then obtained by fitting to a single exponential time.

In Fig. 6a, we see that the average decay time is approximately constant for the range of diameters used. Since the TBC is equal to the product of heat capacity and the inverse decay time, this implies that the TBC scales linearly with the diameter, as the lattice heat capacity. We plot the TBC vs. CNT diameter in Fig. 6b and observe this linear relationship between the TBC and diameter after performing an empirical fit (dashed line). The TBC increases with diameter because a larger diameter means that there are more phonon branches and this implies there are more phonons available to participate in the interfacial thermal transport process. Assuming that the average energy relaxation rate of each phonon mode does not change with diameter, this explains the simple linear scaling of the TBC with diameter over the examined range.

Another measure of heat dissipation from a nanostructure like the CNT is the TBC divided by the diameter, i.e. the TBC per unit area rather than per unit length. Our simulation results suggest that the TBC per unit area with SiO₂ does not vary with diameter for armchair CNTs and is approximately $5.8 \times 10^7 \text{ WK}^{-1}\text{m}^{-2}$ at room temperature. This is a value comparable to that

measured for other (bulk) material interfaces, approximately between that for Pb with diamond, and that for Al with Al_2O_3 .^{29,34} This TBC per unit area is perhaps a more important figure of merit in practical, macroscopic applications such as heat sinks. In this sense, our results indicate that for a given vertical nanotube array packing density (number of nanotubes per unit area) arrays with larger average CNT diameter will benefit from higher thermal conductance at the silicon backside interface, assuming a contact geometry like that depicted in Fig. 1a.

Before concluding, it is also important to compare our simulation results with the few existing experimental studies of the CNT- SiO_2 thermal boundary conductance. A relatively wide range of numbers have been reported for this TBC per unit length.^{9,17-19} From their breakdown studies of CNT devices on SiO_2 , Pop et al^{9,18} extrapolated the TBC to be between 0.12–0.20 $\text{WK}^{-1}\text{m}^{-1}$ for nanotubes between 2–3 nm in diameter. By measuring the temperature distribution in nanotubes of diameter 1.2–2.0 nm with a scanning thermal microscope (SThM), Shi et al¹⁹ obtained TBC values between 0.007–0.06 $\text{WK}^{-1}\text{m}^{-1}$. Finally, from examining the SiO_2 substrate coupling of phonon modes at the Brillouin zone center through Raman thermometry, Steiner et al³⁵ obtained thermal conductance values between 0.03–0.11 $\text{WK}^{-1}\text{m}^{-1}$ for the K, G, and RBM modes of a 1.5 nm diameter CNT. However, given the experimental uncertainties it is challenging to make direct comparison of our simulations with the available data. Nonetheless, our results are well within the experimental range, and in fact help explain why there appear to be a range of values for the TBC with a given substrate, as the variation (and experimental uncertainty) in nanotube diameter naturally leads to variation in the TBC. In addition, the sample-to-sample variability of the CNT-substrate interaction due, for example, to SiO_2 surface roughness or adsorbed species in experiments can also give rise to a significant variability in the empirically extracted values for the TBC.

V. CONCLUSIONS

In summary, we have examined the temperature, diameter, and coupling strength dependence of the thermal boundary conductance (TBC) between carbon nanotubes and amorphous SiO_2 using molecular dynamics simulations. We explored the temperature range $T = 200$ –600 K, nanotube diameter range $D = 0.81$ –1.63 nm, and coupling strength varying by factors $\chi = 1$ –4. Our results show the TBC per unit length is very sensitive to both CNT diameter and interfacial Van der Waals bond strength. The TBC is found to scale linearly with diameter in armchair

CNTs, due to the greater number of phonon modes that can participate in interfacial thermal transport. The TBC scales linearly with the substrate-CNT interaction strength due to the increase in harmonic coupling between CNT and substrate phonon modes. The TBC also increases with temperature as $\sim T^{1/3}$ in the range considered, independently of the substrate-CNT interaction strength.

A simple expression for the CNT-SiO₂ interface thermal coupling per unit length, which is a good approximation to the MD simulation results can be written as

$$G \approx 0.05D\chi \left(\frac{T}{200} \right)^{1/3} \quad (11)$$

where D is in nm and T is in K. With the standard set of parameters $G \approx 0.1 \text{ WK}^{-1}\text{m}^{-1}$ for a 1.7 nm diameter CNT at room temperature, or approximately $5.8 \times 10^7 \text{ WK}^{-1}\text{m}^{-2}$ per unit area. The thermal relaxation time of a single CNT on SiO₂ is found to be independent of diameter, and approximately 85 ps. We note that such MD simulations yield the lattice contribution to thermal transport, which is thought to be dominant due to the much larger heat capacity of phonons at these temperatures. However, future experimental and theoretical work must also examine the role of any electronic degrees of freedom in interfacial thermal transport.

ACKNOWLEDGEMENT

This work has been partly supported by the Nanoelectronics Research Initiative (NRI) SWAN center, the NSF CCF-0829907 grant, and a gift from Northrop Grumman Aerospace Systems (NGAS). The molecular images in Fig. 2, 3 and 5 were generated using the molecular graphics program VMD.³⁶ We acknowledge valuable discussions with Prof. Junichiro Shiomi, and computational support from Reza Toghraee and Prof. Umberto Ravaioli.

REFERENCES

- ¹ S. T. Huxtable, et al., *Nat Mater* **2**, 731 (2003).
- ² R. S. Prasher, X. J. Hu, Y. Chalopin, N. Mingo, K. Lofgreen, S. Volz, F. Cleri, and P. Keblinski, *Physical Review Letters* **102**, 105901 (2009).
- ³ S. Berber, Y.-K. Kwon, and D. Tománek, *Physical Review Letters* **84**, 4613 (2000).
- ⁴ N. Mingo and D. A. Broido, *Physical Review Letters* **95**, 096105 (2005).
- ⁵ N. Mingo and D. A. Broido, *Nano Letters* **5**, 1221 (2005).
- ⁶ B. A. Cola, J. Xu, C. Cheng, X. Xu, T. S. Fisher, and H. Hu, *Journal of Applied Physics* **101**, 054313 (2007).
- ⁷ M. A. Panzer, G. Zhang, D. Mann, X. Hu, E. Pop, H. Dai, and K. E. Goodson, *Journal of Heat Transfer* **130**, 052401 (2008).
- ⁸ S. Hasan, M. A. Alam, and M. S. Lundstrom, *Electron Devices, IEEE Transactions on* **54**, 2352 (2007).
- ⁹ E. Pop, D. A. Mann, K. E. Goodson, and H. Dai, *Journal of Applied Physics* **101**, 093710 (2007).
- ¹⁰ R. Prasher, *Nano Letters* **5**, 2155 (2005).
- ¹¹ R. Prasher, *Applied Physics Letters* **94**, 041905 (2009).
- ¹² C. F. Carlborg, J. Shiomi, and S. Maruyama, *Physical Review B* **78**, 205406 (2008).
- ¹³ T. C. Clancy and T. S. Gates, *Polymer* **47**, 5990 (2006).
- ¹⁴ S. Shenogin, L. Xue, R. Ozisik, P. Keblinski, and D. G. Cahill, *Journal of Applied Physics* **95**, 8136 (2004).
- ¹⁵ M. Hu, P. Keblinski, J.-S. Wang, and N. Raravikar, *Journal of Applied Physics* **104**, 083503 (2008).
- ¹⁶ J. Diao, D. Srivastava, and M. Menon, *The Journal of Chemical Physics* **128**, 164708 (2008).
- ¹⁷ H. Maune, H.-Y. Chiu, and M. Bockrath, *Applied Physics Letters* **89**, 013109 (2006).
- ¹⁸ E. Pop, *Nanotechnology*, 295202 (2008).
- ¹⁹ L. Shi, J. Zhou, P. Kim, A. Bachtold, A. Majumdar, and P. L. McEuen, *Journal of Applied Physics* **105**, 104306 (2009).
- ²⁰ S. Plimpton, *J. Comput. Phys.* **117**, 1 (1995).

²¹ S. J. Stuart, A. B. Tutein, and J. A. Harrison, *The Journal of Chemical Physics* **112**, 6472 (2000).

²² D. W. Brenner, *Physical Review B* **42**, 9458 (1990).

²³ S. Munetoh, T. Motooka, K. Moriguchi, and A. Shintani, *Computational Materials Science* **39**, 334 (2007).

²⁴ J. M. Carpenter and D. L. Price, *Physical Review Letters* **54**, 441 (1985).

²⁵ B. M. Lee, H. K. Baik, B. S. Seong, S. Munetoh, and T. Motooka, *Computational Materials Science* **37**, 203 (2006).

²⁶ T. Hertel, R. E. Walkup, and P. Avouris, *Physical Review B* **58**, 13870 (1998).

²⁷ A. K. Rappe, C. J. Casewit, K. S. Colwell, W. A. Goddard, and W. M. Skiff, *Journal of the American Chemical Society* **114**, 10024 (1992).

²⁸ M. P. Allen and D. J. Tildesley, *Computer simulation of liquids* (Clarendon Press ; Oxford University Press, Oxford [England]; New York, 1989).

²⁹ D. G. Cahill, W. K. Ford, K. E. Goodson, G. D. Mahan, A. Majumdar, H. J. Maris, R. Merlin, and S. R. Phillpot, *Journal of Applied Physics* **93**, 793 (2003).

³⁰ S. Okada, *Chemical Physics Letters* **474**, 302 (2009).

³¹ C.-J. Twu and J.-R. Ho, *Physical Review B* **67**, 205422 (2003).

³² E. T. Swartz and R. O. Pohl, *Reviews of Modern Physics* **61**, 605 (1989).

³³ Z. Xu and M. J. Buehler, *ACS Nano* **3**, 2767 (2009).

³⁴ H.-K. Lyeo and D. G. Cahill, *Physical Review B (Condensed Matter and Materials Physics)* **73**, 144301 (2006).

³⁵ M. Steiner, M. Freitag, V. Perebeinos, J. C. Tsang, J. P. Small, M. Kinoshita, D. Yuan, J. Liu, and P. Avouris, *Nat Nano* **4**, 320 (2009).

³⁶ W. Humphrey, A. Dalke, and K. Schulten, *Journal of Molecular Graphics* **14**, 33 (1996).

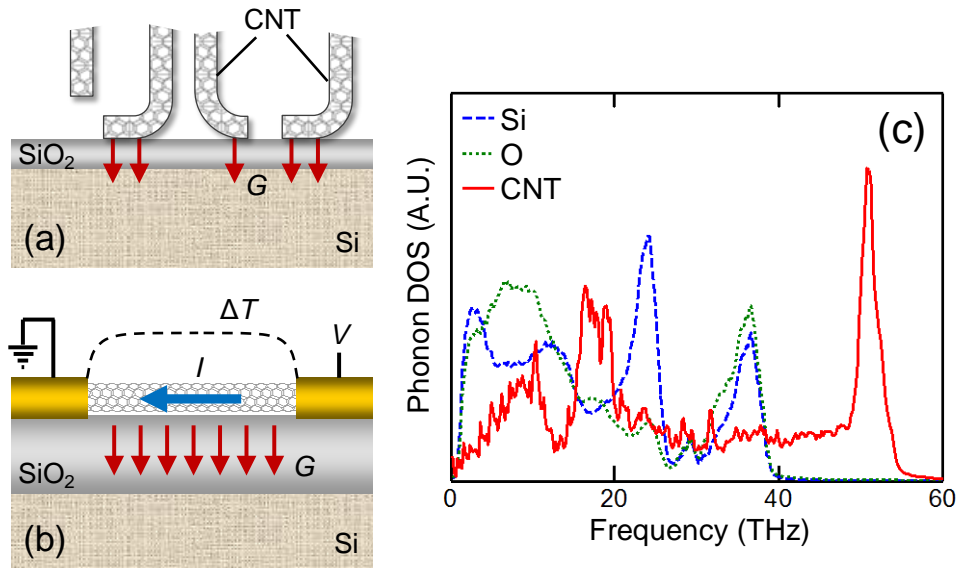


Figure 1: Schematic of heat dissipation from CNTs to SiO₂ in (a) vertical CNT array heat sinks (with native SiO₂ layer on Si wafer),^{6, 7} and in (b) interconnect or transistor applications.^{8, 9} The red arrows show the direction of heat flow, in particular via the CNT-SiO₂ interface. (c) Computed phonon density of states (DOS) in CNT and SiO₂ substrate. The CNT phonon DOS ranges from 0–56 THz, whereas that of Si and O atoms range from 0–40 THz. Between 0–40 THz there is no significant mismatch of the phonon spectra between the CNT and the substrate.

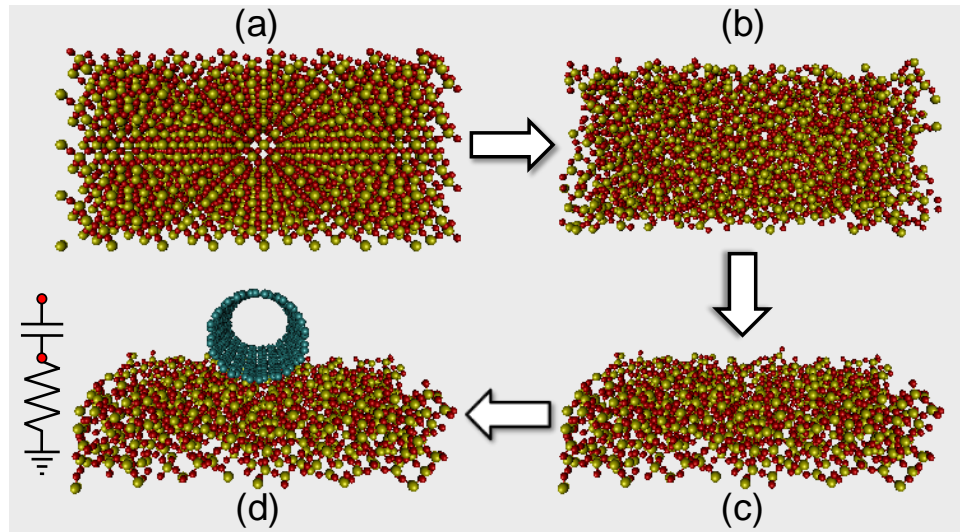


Figure 2: Generating the simulation structure. (a) We start with a crystalline SiO_2 block and anneal it at 6000 K to produce the amorphous SiO_2 domain in (b). (c) We delete the top half of the amorphous block to produce the substrate slab, and then place the CNT on the substrate as in (d). Shown here is a (10,10) nanotube, with substrate coupling strength $\chi = 1$. The inset shows the thermal circuit formed by the CNT heat capacity and the thermal resistance between CNT and substrate ($= 1/G$).

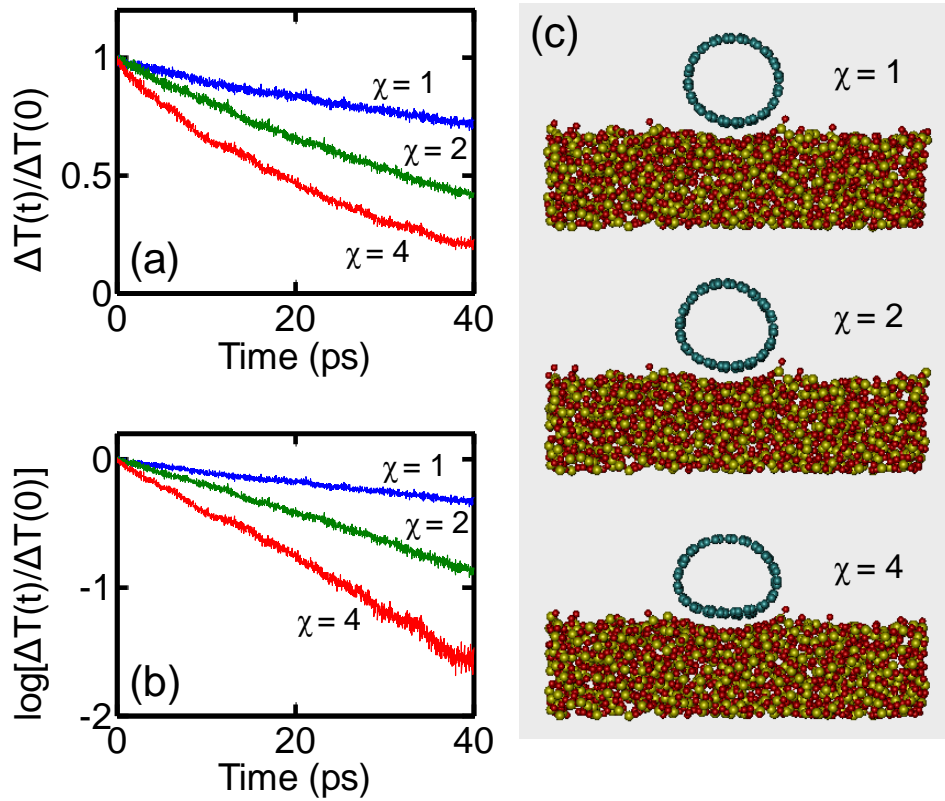


Figure 3: (a) Decay of the normalized CNT-substrate temperature difference at 300 K averaged over 10 runs. (b) Plot of the logarithm of the normalized substrate-CNT temperature difference with respect to time. The decay of the temperature difference can be fitted to a single exponential decay. The decay time is obtained from the negative inverse of the gradient in the first 20 ps. This decay time is used to calculate the TBC, as described in the text. (c) Cross-sectional profiles of a (10,10) CNT for different values of CNT-substrate coupling strength χ . As the CNT-substrate interaction becomes stronger, the CNT profile is deformed, and its cross-section becomes more elliptical.

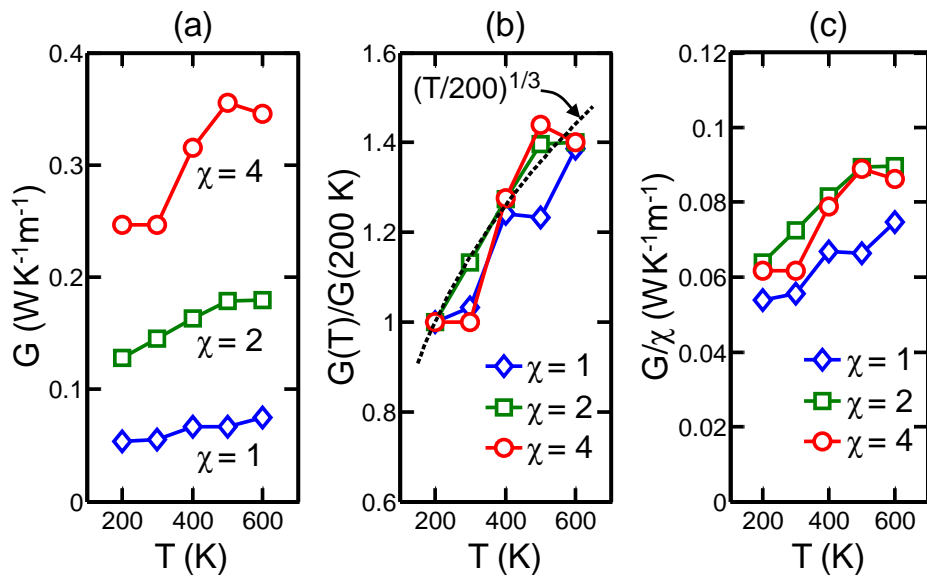


Figure 4: (a) Computed TBC for different values of χ from 200 to 600 K, for the (10,10) CNT with diameter $D = 1.36$ nm. (b) TBC normalized with respect to its value at 200 K. The simulations suggest the TBC varies as $\sim T^{1/3}$ for the range of χ values studied. (c) The TBC normalized with respect to χ . The results suggest there is a direct, nearly linear dependence of the TBC on the strength of the CNT-substrate Van der Waals interaction. This dependence is not captured by conventional theories such as the acoustic or diffuse mismatch models.

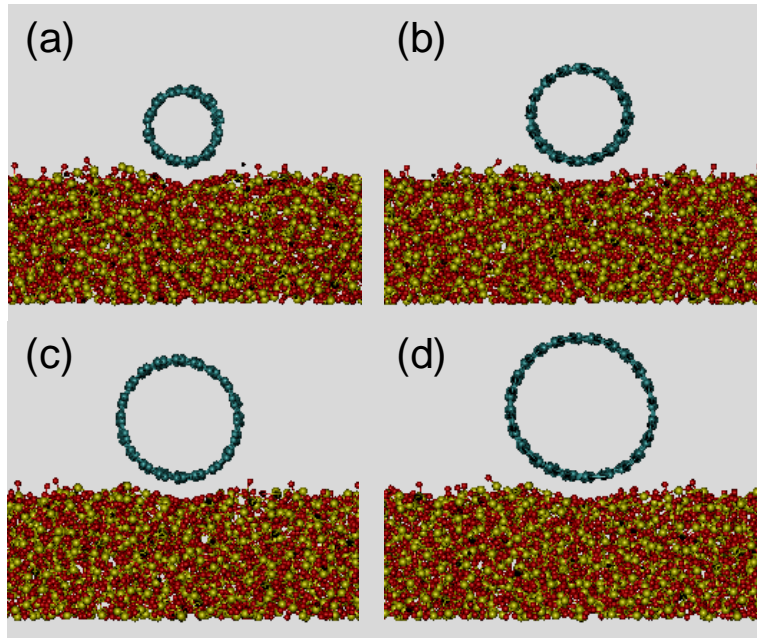


Figure 5: Cross sectional profiles of (a) (6,6), (b) (8,8), (c) (10,10) and (d) (12,12) CNTs on SiO_2 . The corresponding diameters are 0.81, 1.08, 1.36 and 1.63 nm, respectively. The CNT and the substrate are equilibrated at 500 K and 300 K, respectively, before their temperature difference is allowed to decay. Averaging over 10 runs, we extract the decay times and use them to compute the TBC values in Fig. 6.

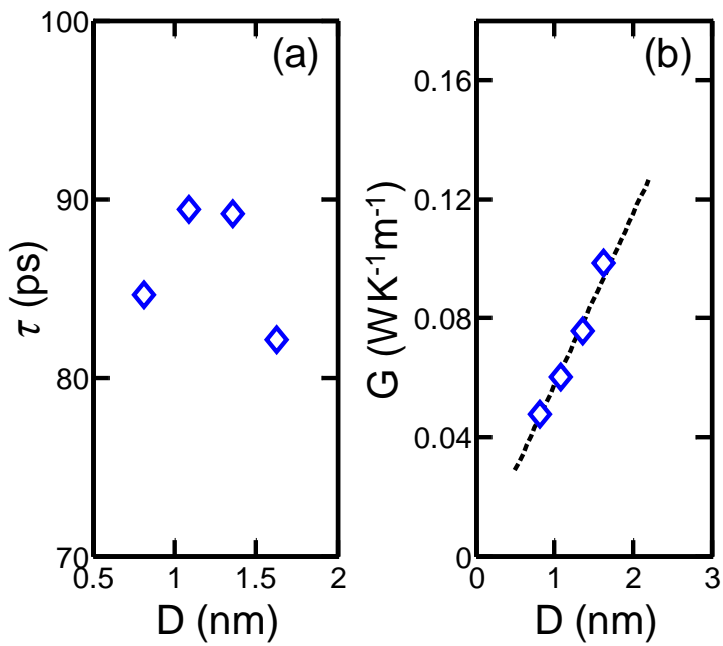


Figure 6: Diameter dependence of the TBC for armchair CNTs. (a) The thermal time constant of a CNT on SiO_2 is roughly constant (~ 85 ps) over the range of diameters considered. (b) The calculated TBC per unit CNT length is approximately proportional to the CNT diameter (dashed line represents linear fit). This implies that the thermal conductance per unit area normalized by the CNT diameter is constant for the range of diameters studied, approximately $5.8 \times 10^7 \text{ WK}^{-1} \text{m}^{-2}$.